A Passive High Altitude Deorbiting Strategy

Charlotte Lücking
Advanced Space Concepts Laboratory, University of Strathclyde
Glasgow G1 1XJ, UK, charlotte.lucking@strath.ac.uk

Supervisors: Colin R. McInnes and Camilla Colombo
Advanced Space Concepts Laboratory, University of Strathclyde

A deorbiting strategy for small satellites, in particular CubeSats, is proposed which exploits the effect of solar radiation pressure to increase the spacecraft orbit eccentricity so that the perigee falls below an altitude where atmospheric drag will cause the spacecraft orbit to naturally decay. This is achieved by fitting the spacecraft with an inflatable reflective balloon. Once this is fully deployed, the overall area-to-mass ratio of the spacecraft is increased; hence solar radiation pressure and aerodynamic drag have a greatly increased effect on the spacecraft orbit. An analytical model of the orbit evolution due to solar radiation pressure and the J_2 effect as a Hamiltonian system shows the evolution of an initially circular orbit. The maximum reachable orbit eccentricity as a function of semi-major axis and area-to-mass ratio can be found and used to determine the size of balloon required for deorbiting from circular orbits of different altitudes. A system design of the device is performed and the feasibility of the proposed deorbiting strategy is assessed and compared to the use of conventional thrusters. The use of solar radiation pressure to increase the orbit eccentricity enables passive deorbiting from significantly higher altitudes than conventional drag augmentation devices.

NOTATION

a	semi-major axis [km]
a_{SRP}	acceleration due to solar rad. pressure [km/s]
α	solar radiation pressure effect parameter
$n_\odot$	average orbital rate of the Earth around the sun [rad/s]
c	speed of light in vacuum [m/s]
c_R	coefficient of reflectivity
e	eccentricity
F_S	solar energy flux density at distance of spacecraft [W/m^2]
J_2	oblateness coefficient of the Earth
μ	gravitational parameter of the Earth [km^3/s^2]
ϕ	in-plane sun-perigee angle [rad]
R_E	average radius of the Earth [km]
σ	spacecraft area-to-mass ratio [m^2/kg]
κ	J_2 effect parameter

1. INTRODUCTION

There is a growing interest in picosatellite projects, in particular CubeSats, whose modest size and standardized launcher interface lowers costs for launch and deployment into orbit. CubeSat missions are typically restricted to Low Earth Orbits (LEO) because of deorbiting requirements. They can be deployed at an altitude where orbit decay due to atmospheric drag can be guaranteed because they characteristically do not accommodate a propulsion system to perform orbital maneuvers. This is due to their small size and simple design which are hard to combine with the complexity of a propulsion system. Moreover, CubeSats are typically launched as a secondary payload together with a significantly larger and more expensive spacecraft. Due to launch safety considerations, storing propellant on the CubeSat would be a hazard for the main payload.

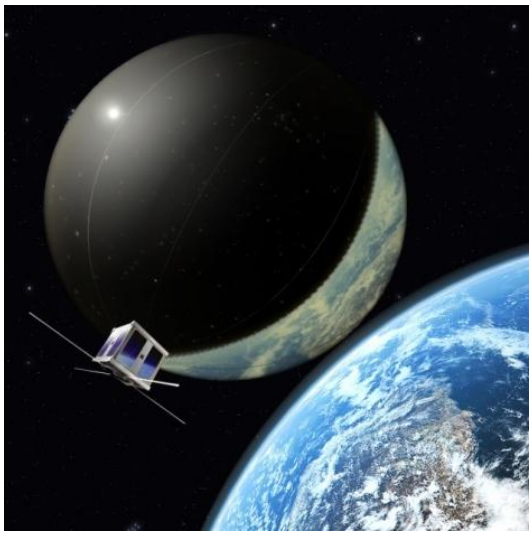

Figure 1: Artist's impression of a CubeSat with deployed reflective deorbiting balloon (image credits: ESA, Aalborg University)

To enable higher altitude CubeSat missions a simple and reliable deorbiting mechanism is needed that does not rely on aerodynamic drag only or the use of propellant for orbit maneuvers. Man-made orbital debris, consisting of obsolete spacecraft and disused launcher parts, is a growing concern for the future of space utilization. In recent years, several guidelines have been published by governmental space agencies and international committees urging the disposal of spacecraft at the end-of-life to avoid the further accumulation of space debris [1]. The preferable method is deorbiting of the satellite at the end of operations. An alternative is to transfer the spacecraft from its operational orbit into a so-called graveyard orbit. The latter option is less satisfactory because the dead satellite, due to external orbit perturbations, could potentially endanger operational satellites. However, a disposal orbit is the only viable option for high altitude spacecraft, when the Δv required for deorbit is too high for conventional propulsion methods [2].

Alternative solutions have been identified which enhance aerodynamic and/or electrodynamic drag [3-8]. The former can be achieved by increasing the area-to-mass ratio (atm) of the spacecraft through the deployment of a large thin-film body. Electrodynamic drag uses the Earth's magnetic field to create a Lorentz force in opposite direction to the spacecraft's velocity by deploying a long, light-weight conductive tether which electrically charges in the ionosphere. Both methods are most effective close to the Earth, increasing the maximum initial orbit altitude from which deorbit can be assured to 600– 1000 km. Beyond this distance both perturbing effects become insignificant.

Previous work has proposed the use of solar radiation pressure for end-of-life maneuvers by rotating the spacecraft's solar panels along the orbit to obtain a secular increase of the semi-major axis. This is achieved by orienting the solar panels to directly face the Sun when moving towards it and parallel to the incoming light when moving away from the Sun to decelerate the spacecraft [9]. This method, however, requires active pointing, thus placing high demands on the durability of the attitude control system and is thus not suitable for a low cost mission.

In this paper a deorbiting method is proposed which exploits the effect of solar radiation pressure (SRP) and Earth oblateness in combination with aerodynamic drag to passively deorbit a satellite within a given time after the end-of-life without any further control requirements. This is achieved by making use of the interaction between SRP and J_2 effect to increase the eccentricity of any initially circular in-plane orbit until the perigee reaches an altitude at which the aerodynamic drag causes the spacecraft to deorbit. The orbital evolution can be divided into two phases as visualized in Figure 2.

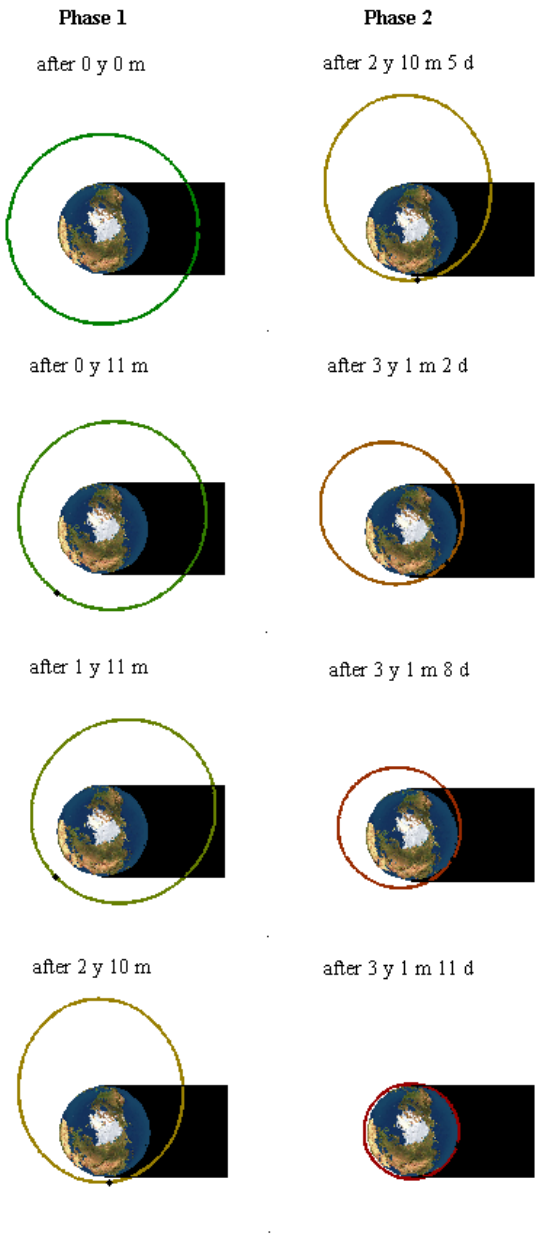

Figure 2: The two phases of the deorbiting maneuver using reflective balloons. In this example the initial orbit altitude is 7000 km and the area-to-mass ratio 3 m^2/kg.

The first phase takes up about 90% of the total maneuver time. In phase one solar radiation pressure is dominant over drag and is

used to increase the orbit eccentricity until drag is the dominant force. Then phase 2 begins in which aerodynamic drag decreases the orbital energy and thus the semi-major axis of the spacecraft and the eccentricity at the same time so that the perigee altitude is kept quasi constant. In the very last days of the maneuver the orbit is quasi circular and at an altitude where drag decreases the orbit rapidly. At this stage the balloon acts in the same way drag-increasing orbit devices would. Solar radiation pressure is now negligible compared to the drag force.

2. ORBITAL DYNAMICS

2.1 Hamiltonian Model

For an orbit which lies in the ecliptic plane and is only perturbed by solar radiation pressure (SRP) and the J_2 effect Krivov and Getino [10] found the expression of the Hamiltonian H which describes the e and ϕ phase space:

$$H = -\sqrt{1-e^2} + \alpha\, e\cos\phi - \frac{\kappa}{3\sqrt{1-e^2}^3} \quad (1)$$

where ϕ is the angle between the direction of the solar radiation and the direction of the orbit perigee from the centre of the Earth. Eq. (1) does not take into account solar eclipses and the tilt of the Earth's axis with respect to the ecliptic plane.

α is a parameter related to the influence of solar radiation pressure on the orbit and κ is related to the J_2 effect:

$$\alpha = \frac{3}{2\,n_{\square}}\, a_{SRP}\sqrt{\frac{a}{\mu}} \quad (2)$$

$$\kappa = \frac{3}{2\;n_{\square}}\; J_2\; R_E^{\,2}\sqrt{\frac{\mu}{a^7}} \quad (3)$$

where a_{SRP} is the acceleration the spacecraft experiences due to solar radiation pressure and can be calculated as:

$$a_{SRP} = c_R\,\frac{F_S}{c}\,\sigma \quad (4)$$

For a spherical spacecraft the area-to-mass ratio σ is not dependent on its attitude. While the parameter κ is only a function of the semi-major axis of the orbit, α is also dependent on the area-to-mass ratio and the coefficient of reflectivity of the spacecraft (c_R).

A typical CubeSat has an atm of less than 0.01 m^2/kg. As such the effect of solar radiation pressure is almost insignificant for the orbit evolution. The inflation of a light-weight balloon, however, can change this dramatically. As can be seen in Figure 3, a 4 m diameter balloon can increase the area-to-mass ratio by a factor of 1000.

For increased area-to-mass ratios the orbital element phase space of e and ϕ exhibits interesting behavior, particularly in the region of 2 - 3 R_E semi-major axis [10].

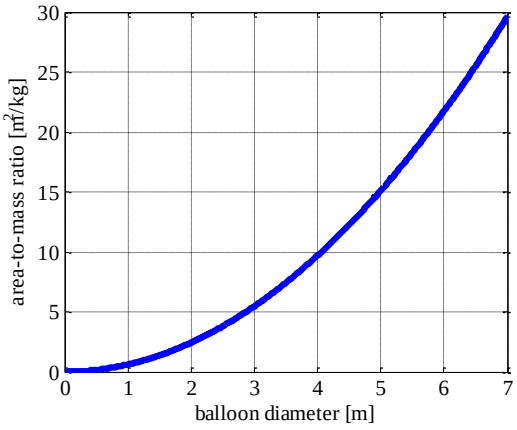

Figure 3: σ as a function of balloon diameter for a total spacecraft mass of 1.3 kg.

For a semi-major axis above approximately 12,350 km the phase space can display one of three behaviors depending on the area-to-mass ratio as shown in Figure 4.

Above a certain σ threshold the maximum eccentricity e_{max} in the evolution of an initially circular orbit can be found at $\phi = 0$ (Figure 4c). At the critical area-to-mass ratio, σ_B, which is dependent on semi-major axis, the evolution of the initially circular orbit bifurcates and passes through a hyperbolic equilibrium at ($e_{B,max}$, π) (Figure 4b) to reach its maximum at ($e_{B,max}$, 0). Below this value of σ, the maximum eccentricity in the evolution of an initially circular orbit can be found at ($e_{1,max}$, 0) (Figure 4a). In the last case, there also appears a second line corresponding to the same value of the Hamiltonian for the initially circular orbit that does not pass through e = 0 and has a minimum at ($e_{2,min}$, π) and a maximum at ($e_{2,max}$, 0). For semi-major axes below circa 12,350 km the behavior always resembles that in Figure 4c.

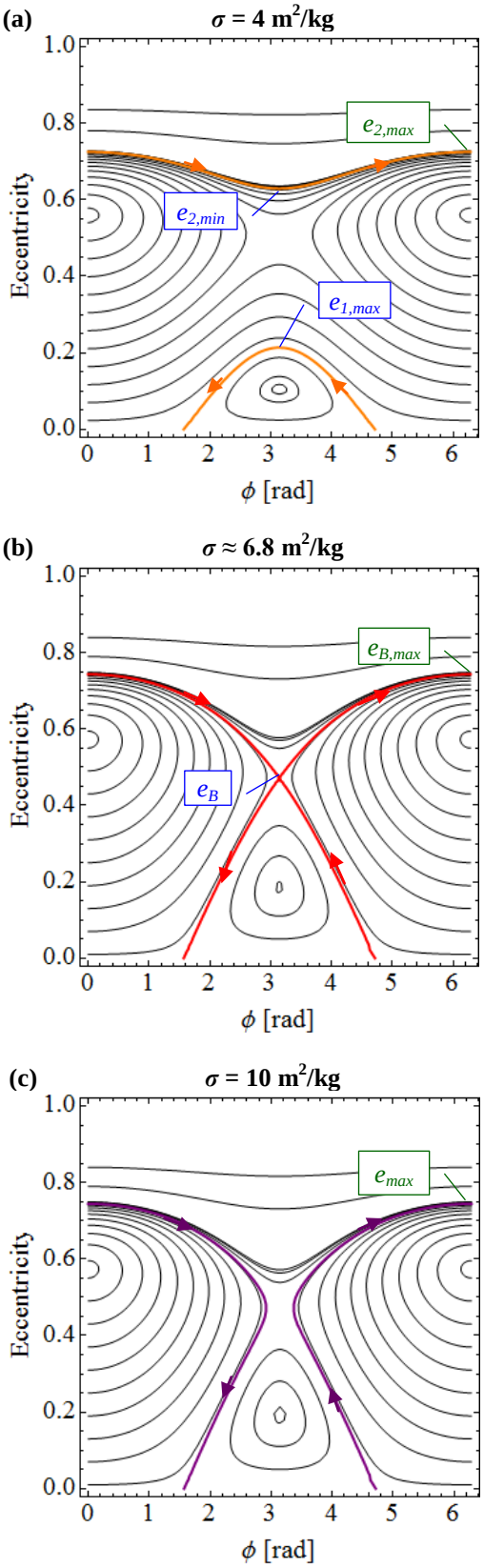

Figure 4: Phase plane diagram for a spacecraft with 15,000 km semi-major axis and a coefficient of reflectivity of c_R = 1.9 for three different values of σ. The bold colored lines indicate the phase line for initial e = 0.

At semi-major axes larger than three Earth's radii the critical area-to-mass ratio, σ_B, and the bifurcation eccentricity, e_B, increase until they become irrelevant for this application and the behavior can always be assumed to resemble Figure 4a.

Figure 5 shows the behavior which occurs depending on semi-major axis and area-to-mass ratio. The line dividing the regions of behavior (a) and behavior (c) is where the bifurcation of the initially circular orbit phase line occurs (b).

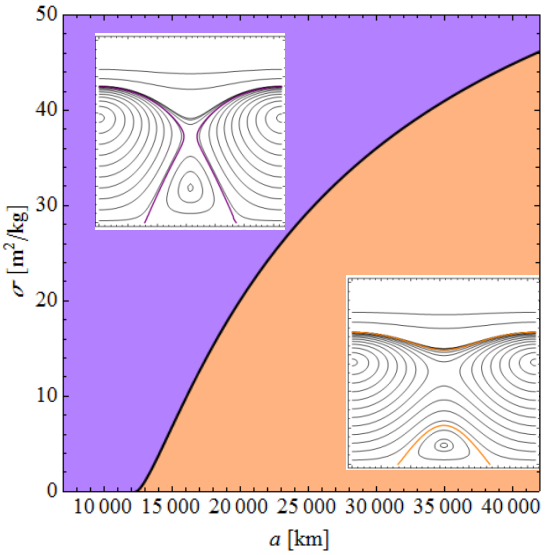

Figure 5: Behavior of the phase space depending on area-to-mass ratio and semi-major axis.

2.2 Required Area-to-Mass Ratio

An expression for the minimum required area-to-mass ratio to deorbit spacecraft on initially circular orbits (e = 0) can be obtained by solving Eq. (1) which results in:

$$H_{circ} = -1 - \frac{\kappa}{3} \tag{5}$$

By inserting Eq. (5) into Eq. (1) and considering that the maximum eccentricity from a circular orbit can be reached at $\phi = \pi$ or $\phi = 0$ (see Figure 4), the resulting equation can be solved to give the required value of α needed to reach a certain eccentricity, e^*, from an initially circular orbit as a function of the semi-major axis:

$$\alpha_1 = \frac{1-\sqrt{1-e^{*2}}}{e^*} + \left(\frac{1}{3e^*} - \frac{1}{3e^*\sqrt{1-e^{*2}}^3}\right)\kappa$$
$$\alpha_2 = -\left(\frac{1-\sqrt{1-e^{*2}}}{e^*} + \left(\frac{1}{3e^*} - \frac{1}{3e^*\sqrt{1-e^{*2}}^3}\right)\kappa\right) \quad (6)$$

The term α_1 corresponds to $\phi = 0$ and α_2 to $\phi = \pi$, the two sun-perigee angles for which the eccentricity can reach its maximum starting from $e = 0$. Since the semi-major axis is given by the spacecraft's circular operational orbit, the required area-to-mass ratio for any c_R can thus be calculated using Eqs. (2) and (4).

Figure 6 shows the solutions of Eq. (6) for a semi-major axis of 15,000 km. The noteworthy eccentricities highlighted in Figure 4 are marked in this diagram. The orange line indicates σ = 4 m²/kg and the purple line indicates σ = 10 m²/kg. The red line is where the phase line for initially circular orbits bifurcates with the critical area-to-mass ratio σ_B corresponding to α_B which is a function of semi-major axis. A problem arises when solving for an . In this case Eq. (6) delivers lower values than α_B, but these correspond to the second identity phase line which never passes through $e = 0$. Thus, to reach values of eccentricity between the hyperbolic equilibrium point (e_B in Figure 4b) and the maximum eccentricity reachable through the bifurcated zero-eccentricity phase line ($e_{B,max}$ in Figure 4b), the minimum area-to-mass ratio solution corresponds to the bifurcated phase plane.

Figure 7 shows the revised function for the required area-to-mass ratio to reach e^* at a = 15,000 km. It is the result of the following decision tree:

(7)

α_B is found through the bifurcating eccentricity $e_B(a)$ which is determined by locating the local extremum in (6) with :

$$\frac{\partial \alpha_{1,2}(a, e_B(a))}{\partial e_B(a)} = 0 \quad (8)$$

$$\alpha_B(a) = \alpha_2(a, e_B(a)) \quad (9)$$

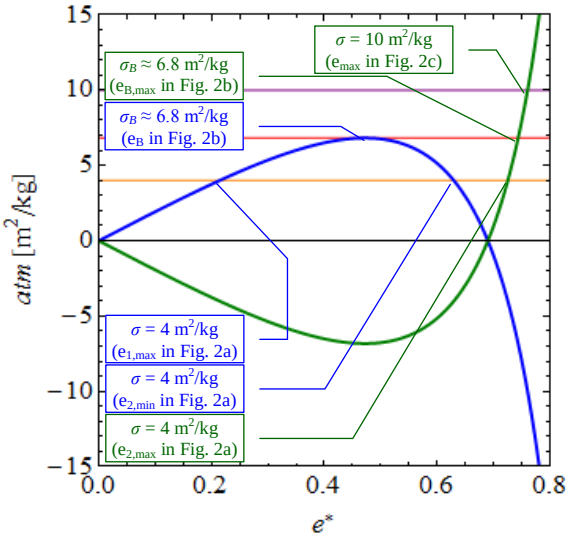

Figure 6: Area-to-mass ratio computed through Eq. (6) with c_R = 1.9 for a semi-major axis of 15,000 km. The blue line represents the case in which the maximum eccentricity can be reached at $\phi = \pi$, the green line the case in which the maximum eccentricity can be reached at $\phi = 0$.

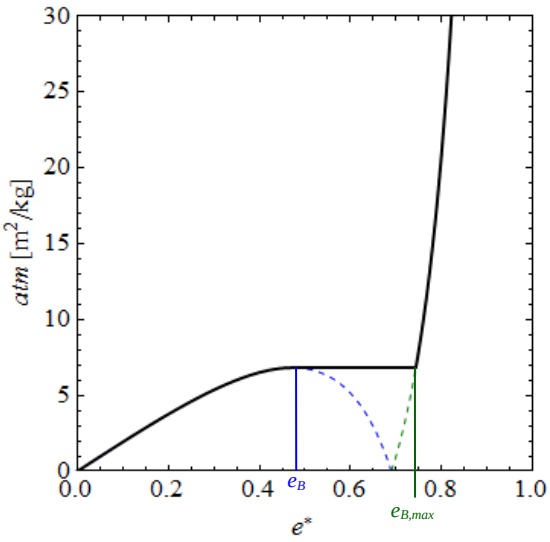

Figure 7: Minimum area-to-mass ratio required to reach eccentricity e^* for a semi-major axis of 15,000 km taking the double identity of the phase line into account (black line). The dashed lines represent the solutions of Eq. (6).

The eccentricity needed to deorbit a spacecraft is called critical eccentricity, e_{crit} and is a function of the semi-major axis and the required perigee altitude, h, to be reached,

(10)

We continue to work with h = 0 km as a worst case assumption, neglecting the effect of drag that, below approximately 600 km altitude, will facilitate the final decay [11]. Both κ and e_{crit} are solely dependent on the initial orbit's semi-major axis. We can therefore determine the minimum area-to-mass ratio required for deorbit as a function of a by substituting $e^* = e_{crit}$ into Eq. (6). Note, however, that this result does not take into any consideration of the transfer time for deorbit. It has already been established that at some semi-major axes the spacecraft orbit would move on a phase plane line which passes through a hyperbolic equilibrium point where it would slow down asymptotically (see Figure 4b). In this case the time covered for transferring the spacecraft from e = 0 to the desired e_{crit} tends to infinity.

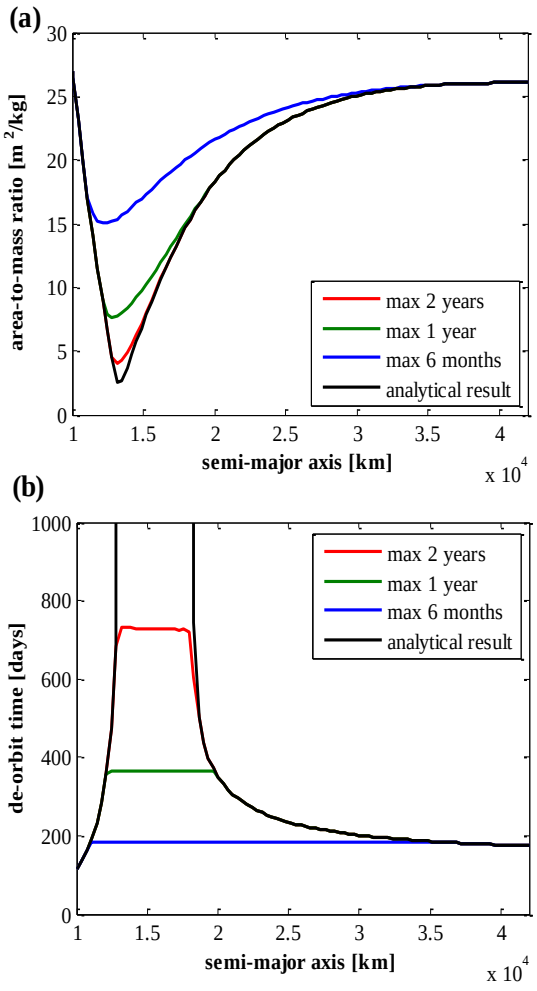

Figure 8: Analytical results (black) compared to results with different maximum deorbiting times restriction imposed. (a) Minimum area-to-mass ratio required for deorbiting and (b) time until deorbiting as a function of semi-major axis.

To find the actual minimum area-to-mass ratio a restriction on the maximum deorbiting time has to be imposed. Figure 8 shows the required area-to-mass ratio for three different maximum deorbiting times, along with the analytical solution (black line). It can be seen that a minimum in required area-to-mass ratio exists for a semi-major axis of about 13,500 km. The lowest value increases significantly for shorter deorbiting times. However, since the device operates completely passively after deployment a longer decay time is not a risk to the success of the deorbiting maneuver.

2.3 Numerical Propagation

In the previous sections only phase 1 of the deorbiting maneuver was investigated (see Figure 2). Two important effects that affect the evolution of an in-plane orbit are not considered in the analytical model: the aerodynamic drag and the eclipses. Both effects are most important when deorbiting from lower initial altitudes. The effect of eclipses is more pronounced here because the part of the orbit shadowed is larger for smaller semi-major axis and the aerodynamic drag is more important because the eccentricity where drag is experienced is the more different from the critical eccentricity defined in the last section the smaller the orbit considered. Considering drag and eclipses makes a Hamiltonian approach impossible. For this reason a numerical analysis was performed and compared to the analytical results.

The numerical evolution of the orbits was performed by using a set of semi-analytical equations which describes the secular and long-periodic change of the orbital elements under the influence of solar radiation pressure, with asymmetry due to eclipses, atmospheric drag [11], and J_2 effect of The Earth's gravity field. The numerical integration of the dynamics equations is performed until the perigee altitudes decrease below 50 km. This is set because below a certain perigee altitude the orbit rapidly decays and the mission is terminated. The numerical integration was performed through an adaptive step-size Runge-Kutta-Fehlberg integration scheme integrator with a six stage pair of approximation of the fourth and fifth order [12], with absolute and relative tolerance of 10^{-11}.

The atmospheric density needed for the drag calculations was interpolated using a scale height model [13].

Figure 9 shows the evolution of orbital elements calculated with the numerical approach for a deorbiting from 7000 km altitude. The two manuoevre phases can be identified easily. In the first phase which lasts about four years in this case the semi-major axis remains close to constant while the eccentricity steadily increases. Then the semi-major axis drops and decreases rapidly until the decay is complete.

Figure 10 shows the results of the numerical propagation in comparison with the analytical results and computations where only aerodynamic drag is considered for a deorbiting within 25 years. The altitude range can be split into three zones: Altitudes below 1250 km where drag is dominant and solar radiation pressure is insignificant, altitudes above 4000 km where the addition of drag and eclipses have only a small effect on the system and the analytical model is valid and the altitudes in between in which the consideration of drag reduces the required area-to-mass ratio significantly.

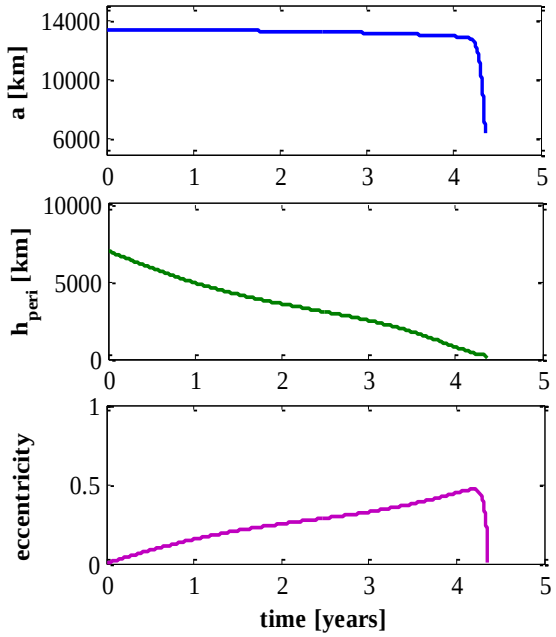

Figure 9: Evolution of semi-major axis, perigee altitude (h_{peri}) and eccentricity during a deorbiting maneuver from a 7000 km altitude circular orbit using with $\sigma = 3$ m^2/kg.

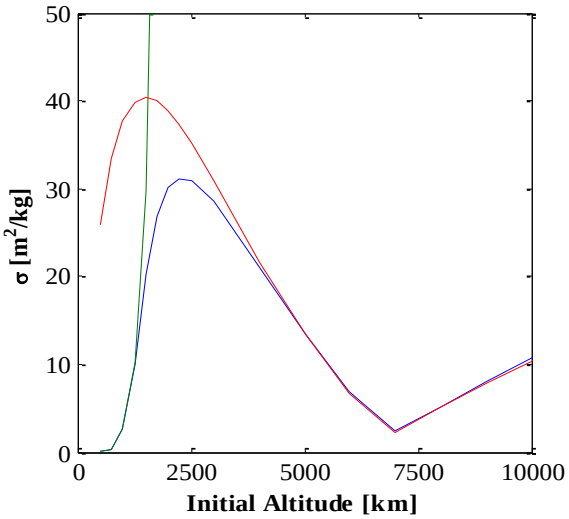

Figure 10: Required area-to-mass-ratio to deorbit within 25 years. Drag only (green), analytical results (red), numerical results (blue).

3. SYSTEM DESIGN

In this section one possible design for a deorbiting subsystem is described. This design was performed to assess the feasibility of the method and to obtain mass and volume ratios of the device as a function of semi-major axis. The aim of the system design is to have a reflective balloon which minimizes stored volume and mass and can be reliably deployed at the end of the mission until the spacecraft can be successfully deorbited. For this three main factors are important: the light-weight reflective balloon material, the deployment mechanism, and the rigidization material and method. The key drivers are reliability, cost and space and mass efficiency.

3.1 Balloon Material

The material chosen for the balloon membrane is a 5 µm aluminized Mylar, which has been impregnated with a rigidizing resin. Mylar has been successfully used in space applications and offers good reliability [14]. This results in a mass of 6.8 g/m^2.

3.2 Deployment

Possible options for deployment include mechanical methods and gas-based inflation, where the gas can be stored in compressed form or be generated in a cold gas generator. A nitrogen gas generator is selected for inflation

of the balloon. This mechanism satisfies the key drivers since it can be manufactured cheaply, is very reliable and mass and volume efficient. For 0.5 g of nitrogen one micro gas generator is required which measures 15 cm^3 and weighs of order 8 g [15]. An inflation pressure of 10^{-4} bar is assumed which leads to one generator per 4.35 m^3 of balloon volume using the ideal gas equation and assuming the nitrogen is at room temperature at inflation. For smaller volumes the balloon can be inflated as a whole. For larger devices the inflation of veins along the surface is suggested.

3.3 Rigidization

Possible methods for the rigidization include shape-memory metals, foams and hardening resins. The latter include resins which harden when coming into contact with UV-light, or when cooled or heated [16]. The disadvantage of many resins is the limited shelf life which is a problem for a device which should last several years before deploying reliably.

The rigidization method chosen is a thermoplastic resin which hardens when cooled. The advantages this resin offers is low mass, unlimited storage time and high reliability [17]. Thermoplastic resins such as polypropylene (PP). PP has a molding temperature T_m of 190 °C and a glass transition temperature T_G of -10 °C. While the balloon is inside the spacecraft it is assumed to be at standard operating temperature (room temperature). At this temperature the resin is very viscuous and stiff. Before the release the device has to be heated to molding temperature. This can be achieved by using solar collectors possibly with added internal heaters. After reaching T_m the balloon will be very flexible and easily deployable. After the deployment it quickly looses heat due to the optical properties of the material. It is highly reflective with an absorptivity of only 0.08 and an emissivity of 0.19 [18].

An ESATAN finite element analysis of the thermal worst case with a constant attitude towards the sun shows the maximum equilibrium surface temperature to be less than -20° C (see Figure 11). The thermal capacity and conductivity of the balloon are very low because of its thin surface. However, the temperature of the sun-facing side is kept close to that of the shadow side by covering the inside of the balloon skin with a black carbon layer which is highly emissive and guarantees a good heat exchange between the sun exposed side and the shadow side of the device.

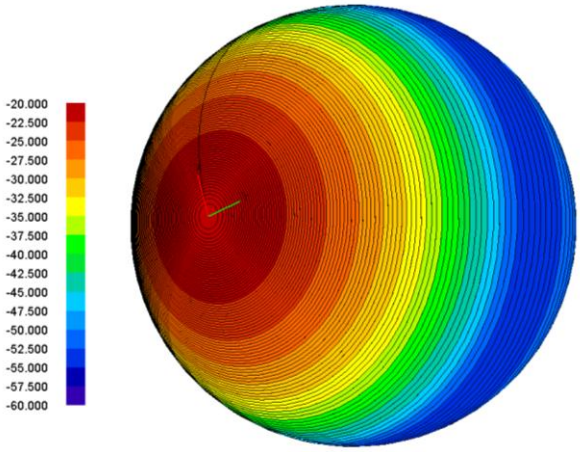

Figure 11: ESATAN temperature results of a worst case steady state analysis.

3.4 Possible Conical Design

The spherical shape of the balloon offers the same cross sectional area at any attitude. The option of using an open cone shape similar to the one proposed by Roberts and Harkness [5] is currently investigated as part of a technology demonstration project carried out by the University of Strathclyde branch of the Students for the Exploration and Development of Space (SEDS), StrathSEDS. A cone shape would greatly reduce the amount of surface material needed. While a sphere has a surface area of four times the cross sectional area for a cone with 90 degree inner angle this factor is only $\sqrt{2}$.

The cone has not got the advantage of a sphere that its visual area is the same from any angle but it is suggested that difference in center of pressure and center of mass in the structure would lead to a passively sun pointing attitude in the absence of aerodynamic drag. [5]

The cone could be deployed and rigidized through struts along the surface and a ring at the top which would make the heating and cooling process required for thermoplastic rigidization unnecessary. The possibility of using phase changing chemicals or shape memory alloys for the deployment are also under investigation.

The prototype for the deorbiting device which is currently being developed is due to be tested in vacuum and microgravity conditions within the next two years. After that an in-orbit demonstration of the method will be aimed at.

3.5 Results

Figure 12 shows the mass ratio of the stowed deorbiting subsystem in relation to the total spacecraft mass calculated using the design parameters described in this section for each the sphere and the cone shape. They are put in comparison with the mass ratio of propellant needed to perform a single impulse maneuver to lower the perigee enough to deorbit assuming a mass-less bi-propellant thruster system. It can be seen that the device is most mass efficient in the Medium Earth Orbit (MEO) regime and has a minimum at an altitude of c. 7000 km.

It can be seen that the spherical design is only feasible in the range of 5,000 to 12,000 km altitude whereas the conical design is superior to the chemical propulsion from an altitude of around 4,000 km upwards. The most efficient region is around 7,000 km with a fraction as low as 2.5%. From an altitude of 20,000 km upwards the required mass fraction changes only slightly and remains at about 20%.

These results have been calculated with the speculative system parameters detailed in this section and are likely to change as the development of the technology demonstrator progresses.

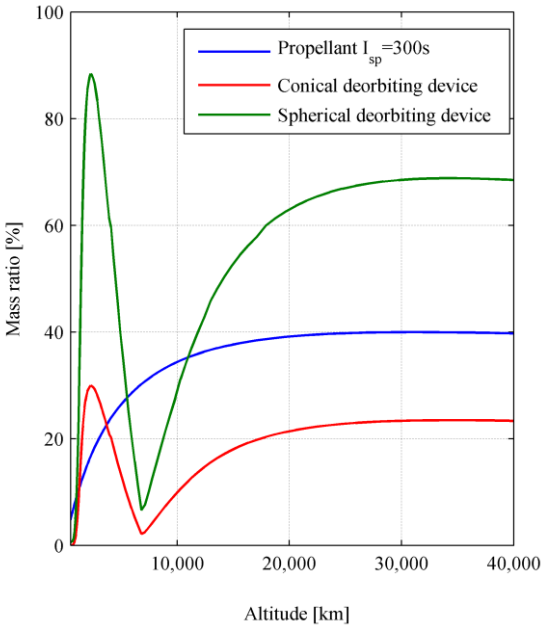

Figure 12: Required mass ratios of the stowed deorbiting balloon for a maximum deorbiting period of 365 days and comparison with mass ratio of propellant only for single impulse maneuver for a bi-propellant thruster system with I_{sp} = 320 s.

4. CONCLUSIONS

The deorbiting strategy presented in this paper has been shown to be a feasible solution for the deorbiting of small satellites in circular low inclination orbits. Using a conical design it is significantly more mass efficient than chemical propulsion-based solutions even at very high altitudes such as geostationary orbits. It is most efficient, however, for altitudes of 1 to 1.5 Earth radii. This orbital regime is commonly known as MEO and of particular importance as the orbits of navigation satellites can be found here.

The use of solar radiation pressure to increase the orbit eccentricity enables passive deorbiting from significantly higher altitudes than conventional drag augmentation devices without any additional risk to the main payload at launch. Additionally this method provides a significant advantage over comparable low-thrust solutions because the deorbiting maneuver will take place completely passively after the deployment of the device. Thus, any damage to the flight systems sustained from traversing the radiation belts cannot affect the reliability of the method.

ACKNOWLEDGMENTS

This work was funded by the European Research Council grant 227571 (VISIONSPACE).

REFERENCES

[1] IADC, IADC Space Debris Mitigation Guidelines. Inter-Agency Space Debris Coordination Committee (2002)

[2] Burkhardt, H., *et al.*, Evaluation of Propulsion Systems for Satellites End-of-Life Deorbiting. 38th AIAA/ASME/SAE/ASEE Joint Propulsion Conference (2002)

[3] Maessen, D. C., *et al.*, Development of a Generic Inflatable Deorbit Device for CubeSats. IAC (2007)

[4] Lappas, V. *et al.*, CubeSail: A low cost CubeSat based solar sail demonstration mission. Advances in Space Research (2011)

[5] Roberts, P. C. E., and Harkness, P. G., Drag Sail for End-of-Life Disposal from Low Earth Orbit. Journal of Spacecraft and Rockets 44, 6, 9 (2007)

[6] Nock, K. T. et al., Balloon device for lowering space object orbits. U.S. Patent 6,830,222 (2004)

[7] Iess, L., et al., Satellite deorbiting by means of electrodynamic tethers part I: General concepts and requirements. *Acta Astronautica* 50 (2002)

[8] Hoyt, R. P., *et al.*, The Terminator Tape: A cost-effective deorbit module for end-of-life disposal of LEO satellites. AIAA Space 2009 Conference and Exposition (2009)

[9] Borja, J. A., and Tun, D., Deorbit process using solar radiation force. *Journal of Spacecraft and Rockets* 43, 685-687 (2006)

[10] Krivov, A. V., and Getino, J., Orbital evolution of high-altitude balloon satellites. *Astronomy and Astrophysics* 318 (1997)

[11] Colombo, C., and McInnes, C., Orbital dynamics of 'smart dust' devices with solar radiation pressure and drag. accepted for publication on *Journal of Guidance, Control, and Dynamics* (2011)

[12] Dormand, J. R., and Prince, P. J., A family of embedded Runge-Kutta formulae. *Journal of computational and applied mathematics* 6, 1, 19-26 (1980)

[13] Vallado, D. A. *Fundamentals of astrodynamics and applications*. New York: Space Technology Library. (2007)

[14] Freeland, R. E., *et al.*, Inflatable Deployable Space Structures Technology Summary. 49th International Astronautical Congress (1998)

[15] Van Der List, M. C. A. M., *et al.*, Applications for solid propellant cool gas generator technology. 4th International Spacecraft Propulsion Conference (2004)

[16] Cadogan, D. P., and Scarborough, S. E., Rigidizable Materials for use in Gossamer Space Inflatable Structures. 42nd AIAA/ ASME/ASCE/AHS/ASC SDM Conference (2001)

[17] Paesano, A., Cohee, D., and Palmese, G. R., Carbon-Fiber Reinforced Thermoplastic Materials for Rigidizable Space Systems. *Journal of Thermoplastic Composite Materials* 16, (2003)

[18] Gilmore, D. G. *Spacecraft Thermal Control Handbook, Volume 1*. American Institute of Aeronautics and Astronautics/Aerospace Press. (2002)